

---

# Deep Koopman Learning using the Noisy Data

---

Wenjian Hao<sup>1\*</sup> Devesh Upadhyay<sup>2</sup> Shaoshuai Mou<sup>1</sup>  
<sup>1</sup>Purdue University <sup>2</sup>Saab, Inc.  
{hao93, mous}@purdue.edu  
devesh.upadhyay@saabinc.com

## Abstract

This paper proposes a data-driven framework to learn a finite-dimensional approximation of a Koopman operator for approximating the state evolution of a dynamical system under noisy observations. To this end, our proposed solution has two main advantages. First, the proposed method only requires the measurement noise to be bounded. Second, the proposed method modifies the existing deep Koopman operator formulations by characterizing the effect of the measurement noise on the Koopman operator learning and then mitigating it by updating the tunable parameter of the observable functions of the Koopman operator, making it easy to implement. The performance of the proposed method is demonstrated on several standard benchmarks. We further compare the presented method with similar methods proposed in the latest literature on Koopman learning.

## 1 Introduction

Directly dealing with complex nonlinear dynamical systems for model-based control design has remained a challenge for the control community. One long standing solution to this problem has been to use linearized models and the associated vast body of knowledge for linear analysis. Linear control theory is a very rich and well-developed field and provides rigorous development of control with methods for providing stability and robustness guarantees. Lyapunov showed that for a linearized system, that is stable around an equilibrium point, there exists a region of stability around this equilibrium point for which the original nonlinear system is also stable [1]. Recent advances in data-driven methods have spurred new and increased research interest in machine learning (ML) based methods for deriving reduced order models (ROM) as surrogates for complex nonlinear systems. This has also led to the adoption of these methods for developing control and autonomy/automation solutions for robotic and unmanned systems. Examples include learning dynamics using deep neural networks (DNNS) [2, 3], Physics informed neural networks (PINNs) [4], and lifting linearization methods such as Koopman operator methods [5–7]. Lifting linearization allows representing a nonlinear system with an equivalent linear system in a lifted, higher dimensional, space. It is, however, typically difficult to find an exact finite dimensional linear representation for most nonlinear systems. Further, the Koopman operator fails on non-autonomous systems:

$$\frac{d\mathbf{x}}{dt} = \mathbf{f}(\mathbf{x}, u, t). \quad (1)$$

This poses a challenge for the control design of dynamical systems in the choice of a sufficient basis function necessary for the lifted system to be linear and exact. Extensions to such systems require truncation-based approximations and the finite-dimensional representation is no longer exact. To this end, various eigen decomposition-based truncations are proposed. In [8] the authors proposed to use deep learning methods to discover the eigenfunctions of the approximated Koopman operator, and [9–12] employed deep neural networks (DNNs) as observable functions of the Koopman operator,

---

\*W. Hao is a PhD student at Purdue University and S. Mou is an associate professor at Purdue University.

which are tuned based on collected state-control pairs by minimizing an appropriately defined loss function which is also referred as the deep Koopman operator method (DKO). Recent work such as [13] has extended the DKO method to approximate nonlinear time-varying systems. Similar to the Koopman operator [14, 15], two other popular methods, dynamic mode decomposition (DMD) [16] and extending dynamic mode decomposition (EDMD) lift the state space to a higher-dimensional space, for which the temporal evolution is approximately linear [17]. These methods rely on a set of measured output variables that collectively define some nonlinear representation of the independent state variables. Establishing a sufficient set of these observable functions remains an active area of research. Further, real-world noisy measurements impose additional challenges. Additionally, for most practical systems, it is also critical to find computationally feasible approximation methods for extracting finite dimensional representations.

**Related work.** While Koopman-based methods have been proven to be effective in learning dynamics from a system’s input-output (state) data pairs. In real-world practical applications, however, the output measurements are noisy and can result in biased estimates of the linear system. Even if the noise of the state variables is assumed to be uncorrelated, the nonlinear transformations in the observables may lead to complex noise-influence correlations between the noise-free states and the transformed observables. Several methods are proposed to solve the measurement noise issue. One solution [18] is to directly measure the states and the observables, this, however, may not always be possible. Noisy measurements are also shown to further complicate the anti-causal observable problem when dealing with the lifting of controlled systems [19].

In other approaches, authors in [20, 21] introduce total least square (TLS) methods in DMD, in [22] the authors propose a combination of the EDMD and TLS methods to account for the measurement noise, and in [23] the authors proposed to solve the EDMD with measurement noise as a robust Koopman operator problem which is a min-max optimization problem.

This paper extends the DKO method to the scenario where the system-states data is corrupted by unknown but bounded measurement noise. As already discussed this creates the challenge of generating additional noise transformations impacted by the DNN-derived basis functions of the deep Koopman operator. This leads to distortion of the noise and the properties of the measurement noise and associated correlations may not remain the same after lifting. The contributions of this work are summarized as follows.

- We propose a data-driven framework to learn the deep Koopman operator from the system states-inputs data pairs under unknown and bounded measurement noise.
- We provide numerical evidence that our proposed method can approximate the system dynamics with reasonable accuracy adequate for control applications.

This paper is organized as follows. Section 2 states the problem. Section 3 presents the proposed algorithm and its theoretical development. Numerical simulations and the comparison of the algorithms are exhibited in Section 4. Finally, Section 5 concludes the paper.

*Notations.* We denote  $\| \cdot \|$  as the Euclidean norm. For a matrix  $A \in \mathbb{R}^{m \times n}$ ,  $\| A \|_F$  denotes its Frobenius norm,  $A'$  denotes its transpose, and  $A^\dagger$  denotes its Moore-Penrose pseudoinverse. Given positive integers  $n$  and  $m$ ,  $\mathbf{I}_n$  denotes the  $n \times n$  identity matrix,  $\mathbf{0}_n \in \mathbb{R}^n$  denotes a vector with all value 0, and  $\mathbf{0}_{n \times m}$  denotes the  $n \times m$  matrix with value 0.

## 2 Problem Setting

Consider the following discrete time-invariant system:

$$\begin{aligned} x_{t+1} &= f(x_t, u_t), & (2) \\ y_t &= x_t + w_t, & (3) \end{aligned}$$

where  $t = 0, 1, 2, \dots$  denotes the time index,  $x_t \in \mathbb{R}^n$  and  $u_t \in \mathbb{R}^m$  denote the system state and control input at time  $t$  respectively,  $y_t \in \mathbb{R}^n$  denotes the measured state at time  $t$ ,  $w_t \in \mathbb{R}^n$  denotes the unknown measurement noise which is assumed to be bounded, i.e.,  $\| w_t \| \leq w_{max}$ , and  $f : \mathbb{R}^n \times \mathbb{R}^m \rightarrow \mathbb{R}^n$  denotes the nonlinear dynamics mapping which is unknown.

Assuming one can observe the measurements-input pairs  $\{(y_t, u_t)\}_{t=0}^T$ , we can create the following data matrices.

$$\begin{aligned} \mathbf{Y} &= [y_0, y_1, \dots, y_{T-1}] \in \mathbb{R}^{n \times T}, & \tilde{\mathbf{Y}} &= [y_1, y_2, \dots, y_T] \in \mathbb{R}^{n \times T}, \\ \mathbf{U} &= [u_0, u_1, \dots, u_{T-1}] \in \mathbb{R}^{m \times T}. \end{aligned} \quad (4)$$

**Deep Koopman learning with noise-free data.** To proceed, we first introduce the deep Koopman operator considering the ideal case when  $w_t = 0$ , that is,  $y_t = x_t$ . The goal of the deep Koopman operator is to find an estimated system dynamics  $\hat{x}_{t+1} = \hat{f}(\hat{x}_t, u_t, \theta_i)$  with  $\hat{x}_0 = x_0$  and  $i = 0, 1, 2, \dots$  denoting the iteration index of  $\theta_i \in \mathbb{R}^p$  such that at any time step  $t$ , for given  $x_t, u_t$  one has  $x_{t+1} = \hat{f}(x_t, u_t, \theta^*)$  by tuning  $\theta_i$ . Here,  $\hat{f}$  is constructed following the Koopman operator theory with a known structure and tunable by parameter  $\theta_i$ , and  $\hat{x}_t \in \mathbb{R}^n$  is the introduced system state for  $\hat{f}$ . More specifically,  $\hat{f}$  is described as

$$g(\hat{x}_{t+1}, \theta_i) = Ag(\hat{x}_t, \theta_i) + Bu_t, \quad (5)$$

$$\hat{x}_{t+1} = Cg(\hat{x}_{t+1}, \theta_i), \quad (6)$$

where  $g(\cdot, \theta_i) : \mathbb{R}^n \times \mathbb{R}^p \rightarrow \mathbb{R}^r$  is usually represented by a deep neural network (DNN) with a known structure and a tunable vector  $\theta_i$ , and we assume the  $g(\cdot, \theta_i)$  is Lipschitz continuous with Lipschitz constant  $L_g$ .  $A \in \mathbb{R}^{r \times r}$ ,  $B \in \mathbb{R}^{r \times m}$ ,  $C \in \mathbb{R}^{n \times r}$  denote the constant matrices to be determined. Here, (5) with  $r \geq n$  represents the dynamics evolution in the lifted space,  $\mathbb{R}^r$  and (6) denotes the projection from the lifted space,  $\mathbb{R}^r$ , to the original space,  $\mathbb{R}^n$ . By combining (5)-(6), one can denote the approximated deep Koopman operator dynamics as follows.

$$\hat{x}_{t+1} = C(Ag(\hat{x}_t, \theta_i) + Bu_t) =: \hat{f}(\hat{x}_t, u_t, \theta_i). \quad (7)$$

Motivated by the recent work [11], one way to achieve such  $\hat{f}$  in (7) that is close to the true dynamics  $f$  in (2) is solving the following double layers optimization problem to minimize the estimation error of  $\frac{1}{T} \sum_{k=0}^{T-1} \|x_{k+1} - \hat{f}(x_k, u_k, \theta_i)\|^2$ .

$$\begin{aligned} \min_{A, B, C} \min_{\theta_i} & \frac{1}{T} \sum_{k=0}^{T-1} \|\delta_k^{lift}\|^2 + \|\delta_k^{origin}\|^2 \\ \text{s.t.} & \quad g(x_{k+1}, \theta_i) = Ag(x_k, \theta_i) + Bu_k + \delta_k^{lift}, \\ & \quad x_{k+1} = Cg(x_{k+1}, \theta_i) + \delta_k^{origin}. \end{aligned} \quad (8)$$

For brevity, we denote the  $g(x_t, \theta_i)$ ,  $A, B, C$  resulting from solving (8) as a set defined as follows.

$$\mathcal{K}_D = \{g(x_k, \theta_i), A, B, C\} \quad (9)$$

which is called a *deep Koopman representation (DKR)* in the remainder of this paper.

**Deep Koopman learning with noisy data.** We now consider the noisy data matrices defined in (4), where  $y_t = x_t + w_t$  with  $w_t \neq \mathbf{0}_n$ ,  $\|w_t\| \leq w_{max}$ . To distinguish the DKR in (9) obtained by solving (8) with  $w_t = 0$ , we introduce the following set to denote the DKR achieved by (8) using the noisy data in (4).

$$\tilde{\mathcal{K}}_D = \{g(y_k, \theta_i), \tilde{A}, \tilde{B}, \tilde{C}\}. \quad (10)$$

Since the difference between  $\mathcal{K}_D$  in (9) and  $\tilde{\mathcal{K}}_D$  in (10) is induced by the measurement noise  $w_t$ , we introduce the following loss function to characterize the difference between the DKRs in (9) and (10).

$$r(\theta_i, w) = \frac{1}{T} \sum_{k=0}^{T-1} \|g(y_k, \theta_i) - g(x_k, \theta_i)\|^2 + \|[\tilde{A}, \tilde{B}] - [A, B]\|_F^2 + \|\tilde{C} - C\|_F^2. \quad (11)$$

By combining (8) with its  $x_k$  replaced by  $y_k$  and (11), we formulate the following min-max problem which first achieves a DKR in (10) from the noisy data in (4) and then corrects the effect of the measurement noise on the DKR (i.e.,  $r(\theta_i, w)$  in (11)) by tuning  $\theta_i$  under the maximum measurement

noise.

$$\begin{aligned}
& \min_{\tilde{A}, \tilde{B}, \tilde{C}} \min_{\theta_i} \max_{w_k} \omega \left\{ \frac{1}{T} \sum_{k=0}^{T-1} \|\tilde{\delta}_k^{lift}\|^2 + \|\tilde{\delta}_k^{origin}\|^2 \right\} + (1 - \omega)r(\theta_i, w) \\
\text{s.t. } & g(y_{k+1}, \theta_i) = \tilde{A}g(y_k, \theta_i) + \tilde{B}u_k + \tilde{\delta}_k^{lift}, \\
& y_{k+1} = \tilde{C}g(y_{k+1}, \theta_i) + \tilde{\delta}_k^{origin}, \\
& r(\theta_i, w) = \frac{1}{T} \sum_{k=0}^{T-1} \|g(y_k, \theta_i) - g(x_k, \theta_i)\|^2 + \|[\tilde{A}, \tilde{B}] - [A, B]\|_F^2 + \|\tilde{C} - C\|_F^2,
\end{aligned} \tag{12}$$

where  $0 < \omega < 1$  denotes the weight. The **problem of interest** is to develop an update rule of  $\theta_i \in \mathbb{R}^p$  using the data matrices in (4) to solve (12).

### 3 Main Results

In this section, we propose an algorithm to solve the problem in (12).

**Key idea.** Since in this paper, the true system states  $x_t$  is not available which makes it impossible to minimize the  $r(\theta_i, w)$  in (11) directly. The key idea of this paper is that we first characterize the  $r(\theta_i, w)$  under the maximum measurement noise  $w_{max}$  only using the observed data matrices in (4), and then we transfer the min-max problem in (12) to a minimization problem using the following proposed theorem.

**Theorem 1** *If the unknown measurement noise  $w_t$  is bounded by  $w_{max}$ , i.e.,  $\|w_t\|^2 \leq w_{max}$ , then the min-max problem of (12) can be reduced to the following minimization problem.*

$$\begin{aligned}
& \min_{\tilde{A}, \tilde{B}, \tilde{C}} \min_{\theta_i} \omega \left\{ \frac{1}{T} \sum_{k=0}^{T-1} \|\tilde{\delta}_k^{lift}\|^2 + \|\tilde{\delta}_k^{origin}\|^2 \right\} + (1 - \omega)\hat{r}(\theta_i) \\
\text{s.t. } & g(y_{k+1}, \theta_i) = \tilde{A}g(y_k, \theta_i) + \tilde{B}u_k + \tilde{\delta}_k^{lift}, \\
& y_{k+1} = \tilde{C}g(y_{k+1}, \theta_i) + \tilde{\delta}_k^{origin}, \\
& \hat{r}(\theta_i) = \frac{1}{T} (\|[\tilde{A}, \tilde{B}]\|_F^2 + \|\tilde{C}\|_F^2 + \|\mathbf{G}\|_F + \|\mathbf{G}\tilde{\mathbf{G}}'\|_F).
\end{aligned} \tag{13}$$

Proof of Theorem 1 is given in Appendix.

#### 3.1 Algorithm

We now present an algorithm that solves (13) using the noisy data in (4). To solve (13), one first needs to write outputs of the DNN into the following compact form.

$$\begin{aligned}
\mathbf{G} &= [g(y_0, \theta), g(y_1, \theta), \dots, g(y_{T-1}, \theta)] \in \mathbb{R}^{r \times T}, \\
\tilde{\mathbf{G}} &= [g(y_1, \theta), g(y_2, \theta), \dots, g(y_T, \theta)] \in \mathbb{R}^{r \times T}.
\end{aligned} \tag{14}$$

Then we rewrite the first layer minimization of (12) using (14) as

$$\begin{aligned}
& \min_{\tilde{A}, \tilde{B}, \tilde{C}} \frac{1}{T} \sum_{k=0}^{T-1} \|g(y_{k+1}, \theta) - (\tilde{A}g(y_k, \theta) + \tilde{B}u_k)\|^2 + \|y_k - \tilde{C}g(y_k, \theta)\|^2 \\
& = \min_{\tilde{A}, \tilde{B}, \tilde{C}} \frac{1}{T} (\|\tilde{\mathbf{G}} - (\tilde{A}\mathbf{G} + \tilde{B}\mathbf{U})\|_F^2 + \|\mathbf{Y} - \tilde{C}\mathbf{G}\|_F^2).
\end{aligned} \tag{15}$$

Here, to ensure there exists a solution of (15), the following assumption is introduced.

**Assumption 1** *The matrices  $\mathbf{G} \in \mathbb{R}^{r \times T}$  and  $\begin{bmatrix} \mathbf{G} \\ \mathbf{U} \end{bmatrix} \in \mathbb{R}^{(r+m) \times T}$  in (15) are with full row ranks.*

**Remark 1** *Assumption 1 is to ensure the matrices  $\mathbf{G} \in \mathbb{R}^{r \times T}$  and  $\begin{bmatrix} \mathbf{G} \\ \mathbf{U} \end{bmatrix} \in \mathbb{R}^{(r+m) \times T}$  are invertible and it naturally requires  $T \geq r + m$ .*

The solution of (15) is given by

$$[\tilde{A}^\theta, \tilde{B}^\theta] = \bar{\mathbf{G}} \begin{bmatrix} \mathbf{G} \\ \mathbf{U} \end{bmatrix}^\dagger, \quad (16)$$

$$\tilde{C}^\theta = \mathbf{Y}\mathbf{G}^\dagger. \quad (17)$$

Here, since the computation of the pseudoinverse of (16)-(17) could be computationally expensive as  $T$  increases, in this paper, we only compute (16)-(17) before updating the  $\theta_i$  to solve the second layer minimization problem. We denote  $\tilde{A}^{\theta_0}$ ,  $\tilde{B}^{\theta_0}$  and  $\tilde{C}^{\theta_0}$  as  $\tilde{A}^\theta$ ,  $\tilde{B}^\theta$  and  $\tilde{C}^\theta$  from (16)-(17) respectively determined by the initial  $\theta_0$ . Finally, the second layer minimization of (13) regarding the parameter  $\theta_i$  is rewritten based on the (16)-(17) as follows.

$$\begin{aligned} \min_{\theta_i \in \mathbb{R}^p} \mathbf{L}_f(\theta_i) = \frac{1}{T} & \left( \left\| \begin{bmatrix} \bar{\mathbf{G}} \\ \mathbf{Y} \end{bmatrix} - \begin{bmatrix} \tilde{A}^{\theta_0} & \tilde{B}^{\theta_0} \\ \tilde{C}^{\theta_0} & \mathbf{0}_{n \times m} \end{bmatrix} \begin{bmatrix} \mathbf{G} \\ \mathbf{U} \end{bmatrix} \right\|_F^2 + \left\| \bar{\mathbf{G}} \begin{bmatrix} \mathbf{G} \\ \mathbf{U} \end{bmatrix}^\dagger \right\|_F^2 + \left\| \mathbf{Y}\mathbf{G}^\dagger \right\|_F^2 + \left\| \mathbf{G} \right\|_F^2 \\ & + \left\| \mathbf{G}\bar{\mathbf{G}}' \right\|_F^2 \right), \end{aligned} \quad (18)$$

To start the algorithm, one first needs to build the DNN  $g(\cdot, \theta_i) : \mathbb{R}^n \times \mathbb{R}^p \rightarrow \mathbb{R}^r$  with non-zero  $\theta_0 \in \mathbb{R}^q$ . Then one can obtain the matrices  $A^{\theta_0} \in \mathbb{R}^{r \times r}$ ,  $B^{\theta_0} \in \mathbb{R}^{r \times m}$  and  $C^{\theta_0} \in \mathbb{R}^{n \times r}$  by computing (16) and (17) respectively based on the observed data matrices in (4) and  $\theta_0$ . Finally, an optimal  $\theta_{\tau+1}$  is obtained by solving (18) through the gradient descent.

To sum up, we have the following algorithm which is named as *deep Koopman learning with the noisy data* (DKND) in the rest of this paper.

---

**Algorithm 1:** Deep Koopman learning with the noisy data (DKND).

---

**Input:**  $\mathbf{Y}$ ,  $\bar{\mathbf{Y}}$ ,  $\mathbf{U}$  in (4).

**Output:**  $g(\cdot, \theta)$ ,  $A$ ,  $B$ ,  $C$ .

**Initialization:** Set the learning rate sequences  $\{\alpha_i\}_{i=0}^S$  and the accuracy  $\epsilon \geq 0$ ; build

$g(\cdot, \theta_i) : \mathbb{R}^n \times \mathbb{R}^p \rightarrow \mathbb{R}^r$  with  $\theta_0 \neq \mathbf{0}_p$ ; compute  $[\tilde{A}^{\theta_0}, \tilde{B}^{\theta_0}]$  and  $\tilde{C}^{\theta_0}$  by solving (16) and (17) respectively using  $\mathbf{Y}$ ,  $\bar{\mathbf{Y}}$ ,  $\mathbf{U}$ , and construct the loss function  $\mathbf{L}_f(\theta_i)$  in (18).

**for**  $i = 0, 1, 2, \dots, S$  **do**

Update the  $\theta_i$  using the following gradient descent.

$$\theta_{i+1} = \theta_i - \alpha_i \left. \frac{d\mathbf{L}_f}{d\theta} \right|_{\theta=\theta_i}.$$

Stop if  $\mathbf{L}_f(\theta_{i+1}) < \epsilon$ .

**end**

---

**Remark 2** Since the loss function  $\mathbf{L}_f(\theta_i)$  in (18) contains the computation of the pseudoinverse regarding the DNN basis function  $g(\cdot, \theta_i)$ , which may lead to the difficulty of computing the gradient of  $\mathbf{L}_f(\theta_i)$ . During the implementation, one way to overcome this issue is to modify the term

$\min_{\theta_i \in \mathbb{R}^p} \left\| \bar{\mathbf{G}} \begin{bmatrix} \mathbf{G} \\ \mathbf{U} \end{bmatrix}^\dagger \right\|_F^2 + \left\| \mathbf{Y}\mathbf{G}^\dagger \right\|_F^2 + \left\| \mathbf{G}\bar{\mathbf{G}}' \right\|_F^2$  in (18) to  $\min_{\theta_i \in \mathbb{R}^p} \left\| \bar{\mathbf{G}} \begin{bmatrix} \mathbf{G} \\ \mathbf{U} \end{bmatrix}' \right\|_F^2 + \left\| \mathbf{Y}\mathbf{G}' \right\|_F^2$  by

following the definition of the Moore–Penrose inverse, i.e., for  $A \in \mathbb{R}^{m \times n}$ , if  $A$  is full row rank, one has  $A^\dagger = A'(AA')^{-1}$ .

## 4 Numerical Simulations

In this subsection, we first demonstrate the performance of the proposed algorithm using one simple linear discrete time-invariant dynamics given by

$$\begin{aligned} x_{t+1} &= \begin{bmatrix} 0.9 & -0.1 \\ 0 & 0.8 \end{bmatrix} x_t + \begin{bmatrix} 0 \\ 1 \end{bmatrix} u_t, \\ y_t &= x_t + w_t \end{aligned} \quad (19)$$

with  $x_t \in \mathbb{R}^2$ ,  $u_t \in \mathbb{R}$ , and  $x_0 = [1, 0]'$ , and cartpole, lunar lander examples from the Openai gym [24], and one unmanned surface vehicles example from [25], and then the comparison between the proposed method and the related methods is conducted.

**Experiment setup.** To conduct the experiment, we first collect the noise-free system states-inputs pairs  $\mathcal{D} = \{(x_t, u_t)\}_{t=0}^T$  from the above examples, where  $u_t$  is randomly generated control inputs following the uniform distribution on  $[0, 1)$  and bounded between  $-1$  and  $1$ . Then we add three types of measurement noise following the Gaussian distribution ( $w_{t,1}$ ), uniform distribution ( $w_{t,2}$ ), and Poisson distribution ( $w_{t,3}$ ) on the collected system states data to achieve the measurements  $y_{t,i} = x_t + w_{t,i}$ ,  $\|w_{t,i}\| \leq \|x_{max}\|$ ,  $i \in \{1, 2, 3\}$ . For brevity, we denote  $\mathcal{D}_i = \{(y_{t,i}, u_t)\}_{t=0}^T$  as the dataset corresponding to the measurement noise  $w_{t,i}$ . Finally, we allocate 80% of  $\mathcal{D}_i$  for training, reserving the remaining 20% for validation.

**Algorithm comparison.** We evaluate the proposed DKND algorithm against three alternative algorithms: DKL which solves (7) with its  $x_k$  substituted by  $y_k$ , DMDTLS from [20], and the multilayer perceptron (MLP) approach. To evaluate the algorithms, for each example, we first construct the DNNs with the same structure and the training and validation datasets remain consistent across methods. To assess the performance of the algorithm, we run all the comparison algorithms for 10 rounds, at each round, we first apply the algorithms to learn the dynamics using the training data from  $\mathcal{D}_i$  and then we evaluate the learned dynamics using both the training data and validation by showing the average estimation error over the 10 rounds denoted by  $e_i$  in the following tables. Specifically, we denote  $e_i^t = \frac{1}{10} \sum_{s=1}^{10} \frac{1}{T_i} \sum_{k=0}^{T_i-1} \|\hat{y}_{k+1,i,s} - x_{k+1}\|^2$  and  $e_i^v = \frac{1}{10} \sum_{s=1}^{10} \frac{1}{T-T_i} \sum_{k=T_i}^{T-1} \|\hat{y}_{k+1,i,s} - x_{k+1}\|^2$  as the estimation error using the training data and validation data respectively, where  $\hat{y}_{k+1,i,s}$  denotes the output of the learned model from any compared approaches with given  $(y_{k,i}, u_k)$  at the  $s$ th round experiment, and  $x_{k+1}$  denotes the collected noise-free system state.

	Methods	Gaussian	Uniform	Poisson
Training data ( $e_i^t$ )	DKND	0.8828	0.4248	1.4305
	DKL	0.9026	0.4571	1.4788
	DMDTLS	4.8390	1.0202	3.5595
	MLP	1.3250	1.1056	1.4887
Validation data ( $e_i^v$ )	DKND	0.7912	0.3848	1.4486
	DKL	0.8311	0.4400	1.4951
	DMDTLS	4.4183	1.1193	3.6040
	MLP	1.2970	1.1919	1.4913

Table 1: 2D example in (19).

	Methods	Gaussian	Uniform	Poisson
Training data ( $e_i^t$ )	DKND	0.7332	1.2596	2.084
	DKL	0.7355	1.2784	2.1211
	DMDTLS	6.1401	29.106	3.2408
	MLP	0.8451	1.2972	2.092
Validation data ( $e_i^v$ )	DKND	0.8089	1.2370	2.0418
	DKL	0.8313	1.2661	2.0975
	DMDTLS	5.8901	29.794	3.5865
	MLP	0.9341	1.2736	2.0375

Table 2: Cartpole.

	Methods	Gaussian	Uniform	Poisson
Training data ( $e_i^t$ )	DKND	0.6748	1.3298	2.1144
	DKL	0.7197	1.4482	2.4453
	DMDTLS	146.2991	41.6894	4.152
	MLP	1.1535	1.4623	2.4103
Validation data ( $e_i^v$ )	DKND	0.5583	1.5176	2.0690
	DKL	0.5357	1.7837	2.4363
	DMDTLS	127.7667	42.9954	4.3466
	MLP	1.0374	1.8381	2.3666

Table 3: Lunar lander.

	Methods	Gaussian	Uniform	Poisson
Training data ( $e_i^t$ )	DKND	1.5021	1.8048	7.3000
	DKL	1.3714	1.8350	7.5998
	DMDTLS	42.6629	28.444	225.3986
	MLP	1.3363	1.7036	7.2282
Validation data ( $e_i^v$ )	DKND	6.8964	5.9763	7.1395
	DKL	15.4834	11.6304	8.0383
	DMDTLS	48.4859	29.4132	231.5419
	MLP	8.5826	9.0678	7.3324

Table 4: The unmanned surface vehicle.

**Results analysis.** As shown in Tables 1-4, the proposed DKND method provides smaller prediction errors compared to the DKL method and DMDTLS method under the three types of measurement noise on the benchmark environments. In the Cartpole example, the DKND has a similar performance as the MLP method under the Poisson noise. Due to the page limitation, we provide a detailed comparison between the DKL and DKND methods and the details of the experiment such as the measurement noise generation, the DNNs structures, and training parameters in the Appendix.

## 5 Discussion and conclusions

In this paper, we proposed a data-driven framework named deep Koopman learning with noisy data (DKND) to address the problem of learning the system dynamics from the data with measurement noise. Here, by learning dynamics we mean learning an estimated dynamics that given  $y_t, u_t$  the output of the estimated dynamics  $\hat{y}_{t+1}$  is close to the true system state  $x_{t+1}$  with reasonable accuracy. The key contribution is that the proposed approach modifies the existing deep Koopman problem by characterizing the noise effect on the learned deep Koopman representation in (9) and reducing it by tuning the DNNs parameter to minimize (13) which only requires the unknown measurement noise to be bounded. We show the algorithm performance by comparing it with related methods on the datasets with three different types of measurement noises using one simple 2D dynamics, cartpole, lunar lander, and one surface vehicle example.

**Limitations.** Since the formulation of this paper only considers the scenario where the measurement noise is with a known upper bound, the effect of the noise bound on the proposed method remains to be formally researched. Besides that, the DKND can only achieve the local minimum due to the non-convexity of the DNN. Some future work including how to design the optimal control based on the learned dynamics with the measured system states needs to be studied.

## References

- [1] A.Lyapunov. The general problem of the stability of motion. *International Journal of Control*, 55(3), 1992.
- [2] Kevin Patrick Murphy. *Dynamic bayesian networks: representation, inference and learning*. University of California, Berkeley, 2002.
- [3] Morgan T Gillespie, Charles M Best, Eric C Townsend, David Wingate, and Marc D Killpack. Learning nonlinear dynamic models of soft robots for model predictive control with neural networks. In *2018 IEEE International Conference on Soft Robotics (RoboSoft)*, pages 39–45. IEEE, 2018.
- [4] Maziar Raissi, Paris Perdikaris, and George E Karniadakis. Physics-informed neural networks: A deep learning framework for solving forward and inverse problems involving nonlinear partial differential equations. *Journal of Computational Physics*, 378:686–707, 2019.
- [5] Igor Mezić. On applications of the spectral theory of the koopman operator in dynamical systems and control theory. In *2015 54th IEEE Conference on Decision and Control (CDC)*, pages 7034–7041. IEEE, 2015.

- [6] Joshua L Proctor, Steven L Brunton, and J Nathan Kutz. Generalizing koopman theory to allow for inputs and control. *SIAM Journal on Applied Dynamical Systems*, 17(1):909–930, 2018.
- [7] Alexandre Mauroy and Jorge Goncalves. Linear identification of nonlinear systems: A lifting technique based on the koopman operator. In *2016 IEEE 55th Conference on Decision and Control (CDC)*, pages 6500–6505. IEEE, 2016.
- [8] Bethany Lusch, Steven L Brunton, and J Nathan Kutz. Data-driven discovery of koopman eigenfunctions using deep learning. *Bulletin of the American Physical Society*, 2017.
- [9] Enoch Yeung, Soumya Kundu, and Nathan Hodas. Learning deep neural network representations for koopman operators of nonlinear dynamical systems. In *2019 American Control Conference (ACC)*, pages 4832–4839. IEEE, 2019.
- [10] Bethany Lusch, J Nathan Kutz, and Steven L Brunton. Deep learning for universal linear embeddings of nonlinear dynamics. *Nature communications*, 9(1):1–10, 2018.
- [11] Yiqiang Han, Wenjian Hao, and Umesh Vaidya. Deep learning of koopman representation for control. In *2020 59th IEEE Conference on Decision and Control (CDC)*, pages 1890–1895. IEEE, 2020.
- [12] Petar Bevanda, Max Beier, Sebastian Kerz, Armin Lederer, Stefan Sosnowski, and Sandra Hirche. Koopmanizingflows: Diffeomorphically learning stable koopman operators. *arXiv preprint arXiv:2112.04085*, 2021.
- [13] Wenjian Hao, Bowen Huang, Wei Pan, Di Wu, and Shaoshuai Mou. Deep koopman learning of nonlinear time-varying systems. *Automatica*, 159:111372, 2024.
- [14] Bernard O Koopman. Hamiltonian systems and transformation in hilbert space. *Proceedings of the national academy of sciences of the united states of america*, 17(5):315, 1931.
- [15] Bernard O Koopman and J v Neumann. Dynamical systems of continuous spectra. *Proceedings of the National Academy of Sciences*, 18(3):255–263, 1932.
- [16] Peter J Schmid. Dynamic mode decomposition of numerical and experimental data. *Journal of fluid mechanics*, 656:5–28, 2010.
- [17] Milan Korda and Igor Mezić. Linear predictors for nonlinear dynamical systems: Koopman operator meets model predictive control. *Automatica*, 93:149–160, 2018.
- [18] Filippos E Sotiropoulos. *Methods for Control in Robotic Excavation*. MIT Dissertation, Cambridge, 2021.
- [19] Nicholas Stearns Selby. *On the Application of Machine Learning and Physical Modeling Theory to Causal Lifting Linearizations of Nonlinear Dynamical Systems with Exogenous Input and Control*. MIT Dissertation, Cambridge, 2021.
- [20] Scott TM Dawson, Maziar S Hemati, Matthew O Williams, and Clarence W Rowley. Characterizing and correcting for the effect of sensor noise in the dynamic mode decomposition. *Experiments in Fluids*, 57:1–19, 2016.
- [21] Maziar S Hemati, Clarence W Rowley, Eric A Deem, and Louis N Cattafesta. De-biasing the dynamic mode decomposition for applied koopman spectral analysis of noisy datasets. *Theoretical and Computational Fluid Dynamics*, 31:349–368, 2017.
- [22] Masih Haseli and Jorge Cortés. Approximating the koopman operator using noisy data: noise-resilient extended dynamic mode decomposition. In *2019 American Control Conference (ACC)*, pages 5499–5504. IEEE, 2019.
- [23] Subhrajit Sinha, Sai P Nandanoori, and DA Barajas-Solano. Online real-time learning of dynamical systems from noisy streaming data. *Scientific Reports*, 13(1):22564, 2023.
- [24] Greg Brockman, Vicki Cheung, Ludwig Pettersson, Jonas Schneider, John Schulman, Jie Tang, and Wojciech Zaremba. Openai gym. *arXiv preprint arXiv:1606.01540*, 2016.
- [25] Brian Bingham, Carlos Agüero, Michael McCarrin, Joseph Klamo, Joshua Malia, Kevin Allen, Tyler Lum, Marshall Rawson, and Rumman Waqar. Toward maritime robotic simulation in gazebo. In *OCEANS 2019 MTS/IEEE SEATTLE*, pages 1–10. IEEE, 2019.



## A Appendix / supplemental material

### A.1 Proof of Theorem 1.

Before we present the proof, the following notions are introduced. First we let

$$\delta g_t = g(y_t, \theta) - g(x_t, \theta)$$

and due to the assumption that  $\|w_t\| \leq w_{max}$  and  $g(\cdot, \theta)$  is Lipschitz continuous we can have  $\|\delta g_t\| \leq L_g w_{max}$ . We then introduce the following data matrices.

$$\begin{aligned} \Delta \mathbf{G} &= [\delta g_0, \delta g_1, \dots, \delta g_{T-1}] \in \mathbb{R}^{r \times T}, \Delta \bar{\mathbf{G}} = [\delta g_1, \delta g_2, \dots, \delta g_T] \in \mathbb{R}^{r \times T}, \\ \mathbf{G}_x &= [g(x_0, \theta), g(x_1, \theta), \dots, g(x_{T-1}, \theta)] \in \mathbb{R}^{r \times T}, \\ \bar{\mathbf{G}}_x &= [g(x_1, \theta), g(x_2, \theta), \dots, g(x_T, \theta)] \in \mathbb{R}^{r \times T}, \\ \mathbf{X} &= [x_0, x_1, \dots, x_{T-1}] \in \mathbb{R}^{n \times T}, \bar{\mathbf{X}} = [x_1, x_2, \dots, x_T] \in \mathbb{R}^{n \times T}, \\ \mathbf{W} &= [w_0, w_1, \dots, w_{T-1}] \in \mathbb{R}^{n \times T}, \bar{\mathbf{W}} = [w_1, w_2, \dots, w_T] \in \mathbb{R}^{n \times T}, \end{aligned} \quad (20)$$

From (14) and (20), one has

$$\begin{aligned} \mathbf{Y} &= \mathbf{X} + \mathbf{W}, \quad \bar{\mathbf{Y}} = \bar{\mathbf{X}} + \bar{\mathbf{W}}, \\ \mathbf{G} &= \mathbf{G}_x + \Delta \mathbf{G}, \quad \bar{\mathbf{G}} = \bar{\mathbf{G}}_x + \Delta \bar{\mathbf{G}}. \end{aligned} \quad (21)$$

We start from the first layer minimization of (12), of which the solution is given in (16)-(17). By using the notations in (20), one has the following dynamics matrices  $A, B, C$  of the DKR in (9) with  $w_t = 0$  by rewriting (16)-(17).

$$[A^\theta, B^\theta] = \bar{\mathbf{G}}_x \begin{bmatrix} \mathbf{G}_x \\ \mathbf{U} \end{bmatrix}^\dagger, \quad (22)$$

$$C^\theta = \mathbf{X} \mathbf{G}_x^\dagger. \quad (23)$$

We then expand the (22)-(23) using the notation in (21) and the Sherman–Morrison formula, that is, for given invertible matrix  $A \in \mathbb{R}^{n \times n}$  and column vectors  $n, v \in \mathbb{R}^n$ , if  $1 + v^T A^{-1} u \neq 0$ , one has

$$(A + uv^T)^{-1} = A^{-1} - \frac{A^{-1}uv^T A^{-1}}{1 + v^T A^{-1}u}.$$

It leads to

$$\begin{aligned} & [A^\theta, B^\theta] \\ &= \bar{\mathbf{G}}_x \begin{bmatrix} \mathbf{G}_x \\ \mathbf{U} \end{bmatrix}^\dagger = (\bar{\mathbf{G}} - \Delta \bar{\mathbf{G}}) \begin{bmatrix} \mathbf{G} - \Delta \mathbf{G} \\ \mathbf{U} \end{bmatrix}^\dagger \\ &= (\bar{\mathbf{G}} - \Delta \bar{\mathbf{G}}) \begin{bmatrix} \mathbf{G} - \Delta \mathbf{G} \\ \mathbf{U} \end{bmatrix}' \left( \begin{bmatrix} \mathbf{G} - \Delta \mathbf{G} \\ \mathbf{U} \end{bmatrix} \begin{bmatrix} \mathbf{G} - \Delta \mathbf{G} \\ \mathbf{U} \end{bmatrix}' \right)^{-1} \\ &= (\bar{\mathbf{G}} \begin{bmatrix} \mathbf{G} \\ \mathbf{U} \end{bmatrix}' - \underbrace{[\bar{\mathbf{G}} - \Delta \bar{\mathbf{G}}, \Delta \bar{\mathbf{G}}]}_{\mathbf{n}} \begin{bmatrix} \Delta \mathbf{G}' & 0 \\ \mathbf{G}' & \mathbf{U}' \end{bmatrix}) \underbrace{\left( \begin{bmatrix} \mathbf{G} \\ \mathbf{U} \end{bmatrix} \begin{bmatrix} \mathbf{G} \\ \mathbf{U} \end{bmatrix}' \right)}_{\mathbf{p}}^{-1} \\ &+ \underbrace{\begin{bmatrix} \Delta \mathbf{G} - \mathbf{G} & -\Delta \mathbf{G} \\ -\mathbf{U} & 0 \end{bmatrix}}_{\mathbf{u}} \underbrace{\begin{bmatrix} \Delta \mathbf{G}' & 0 \\ \mathbf{G}' & \mathbf{U}' \end{bmatrix}}_{\mathbf{v}'}^{-1} \\ &= [\tilde{A}^\theta, \tilde{B}^\theta] + (\mathbf{n} \mathbf{v}' \mathbf{p}^{-1} - [\tilde{A}^\theta, \tilde{B}^\theta]) \mathbf{u} \mathbf{v}' \mathbf{p}^{-1} (\mathbf{I} + \mathbf{v}' \mathbf{p}^{-1} \mathbf{u})^{-1} - \mathbf{n} \mathbf{v}' \mathbf{p}^{-1} \end{aligned} \quad (24)$$

and

$$\begin{aligned} C^\theta &= \mathbf{X} \mathbf{G}_x^\dagger = (\mathbf{Y} - \mathbf{W})(\mathbf{G} - \Delta \mathbf{G})^\dagger, \\ &= (\mathbf{Y} - \mathbf{W})(\mathbf{G} - \Delta \mathbf{G})' ((\mathbf{G} - \Delta \mathbf{G})(\mathbf{G} - \Delta \mathbf{G})')^{-1}, \\ &= (\mathbf{Y} \mathbf{G}' - \underbrace{[\mathbf{Y} + \mathbf{W}, -\mathbf{W}]}_{\bar{\mathbf{n}}} \begin{bmatrix} \Delta \mathbf{G}' \\ \mathbf{G}' \end{bmatrix}) \underbrace{(\mathbf{G} \mathbf{G}')}_{\bar{\mathbf{p}}} + \underbrace{[-\mathbf{G} + \Delta \mathbf{G}, -\Delta \mathbf{G}]}_{\bar{\mathbf{u}}} \underbrace{\begin{bmatrix} \Delta \mathbf{G}' \\ \mathbf{G}' \end{bmatrix}}_{\bar{\mathbf{v}'}}^{-1} \\ &= \tilde{C}^\theta + (\bar{\mathbf{n}} \bar{\mathbf{v}}' \bar{\mathbf{p}}^{-1} - \tilde{C}^\theta) \bar{\mathbf{u}} \bar{\mathbf{v}}' \bar{\mathbf{p}}^{-1} (\mathbf{I} + \bar{\mathbf{v}}' \bar{\mathbf{p}}^{-1} \bar{\mathbf{u}})^{-1} - \bar{\mathbf{n}} \bar{\mathbf{v}}' \bar{\mathbf{p}}^{-1}. \end{aligned} \quad (25)$$

We recall the following from (12).

$$r(\theta_i, w) = \frac{1}{T} \sum_{k=0}^{T-1} \|\delta g_k\| + \|[\tilde{A}^\theta, \tilde{B}^\theta] - [A^\theta, B^\theta]\|_F + \|\tilde{C}^\theta - C^\theta\|_F.$$

From (24)-(25) one has

$$\begin{aligned} & \frac{1}{T} \sum_{k=0}^{T-1} \|\delta g_k\| + \|[\tilde{A}^\theta, \tilde{B}^\theta] - [A^\theta, B^\theta]\|_F + \|\tilde{C}^\theta - C^\theta\|_F \\ &= \frac{1}{T} \sum_{k=0}^{T-1} \|\delta g_k\| + \|(\mathbf{nv}'\mathbf{p}^{-1} - [\tilde{A}^\theta, \tilde{B}^\theta])\mathbf{uv}'\mathbf{p}^{-1}(\mathbf{I} + \mathbf{v}'\mathbf{p}^{-1}\mathbf{u})^{-1} + \mathbf{nv}'\mathbf{p}^{-1}\|_F \\ & \quad + \|(\bar{\mathbf{n}}\bar{\mathbf{v}}' - \tilde{C}^\theta)\bar{\mathbf{u}}\bar{\mathbf{v}}'\bar{\mathbf{p}}^{-1}(\mathbf{I} - \bar{\mathbf{v}}'\bar{\mathbf{p}}^{-1}\bar{\mathbf{u}})^{-1} + \bar{\mathbf{n}}\bar{\mathbf{v}}'\bar{\mathbf{p}}^{-1}\|_F \end{aligned} \quad (26)$$

Then let  $\mathbf{nv}'\mathbf{p}^{-1} = [\tilde{A}^\theta, \tilde{B}^\theta]$  and  $\bar{\mathbf{n}}\bar{\mathbf{v}}'\bar{\mathbf{p}}^{-1} = \tilde{C}^\theta$ , (26) becomes

$$r(\theta_i, w) = \frac{1}{T} \sum_{k=0}^{T-1} \|\delta g_k\| + \|[\tilde{A}^\theta, \tilde{B}^\theta]\|_F + \|\tilde{C}^\theta\|_F. \quad (27)$$

Here to achieve

$$\mathbf{nv}'\mathbf{p}^{-1} = [\tilde{A}^\theta, \tilde{B}^\theta] = \bar{\mathbf{G}} \begin{bmatrix} \mathbf{G} \\ \mathbf{U} \end{bmatrix}' \mathbf{p}^{-1}$$

and

$$\bar{\mathbf{n}}\bar{\mathbf{v}}'\bar{\mathbf{p}}^{-1} = \tilde{C}^\theta = \mathbf{Y}\mathbf{G}'\bar{\mathbf{p}}^{-1},$$

one can formulate the following loss function by adding the extra feature functions in (26), which share the same optimal solution as (26).

$$\begin{aligned} & \hat{r}(\theta) \\ &= \frac{1}{T} \sum_{k=0}^{T-1} \|\delta g_k\| + \|[\tilde{A}^\theta, \tilde{B}^\theta]\|_F + \|\tilde{C}^\theta\|_F + \frac{1}{T} (\|\bar{\mathbf{n}}\bar{\mathbf{v}}' - \mathbf{Y}\mathbf{G}'\|_F + \|\mathbf{nv}' - \bar{\mathbf{G}} \begin{bmatrix} \mathbf{G} \\ \mathbf{U} \end{bmatrix}'\|_F) \\ &= \frac{1}{T} \sum_{k=0}^{T-1} \|\delta g_k\| + \frac{1}{T} (\|(\mathbf{Y} - \mathbf{W})(\mathbf{G} - \Delta\mathbf{G})'\|_F + \|(\bar{\mathbf{G}} - \Delta\bar{\mathbf{G}}) \begin{bmatrix} \mathbf{G} \\ \mathbf{U} \end{bmatrix}'\|_F) \\ & \quad + \|[\tilde{A}^\theta, \tilde{B}^\theta]\|_F + \|\tilde{C}^\theta\|_F. \end{aligned} \quad (28)$$

Note here that the minimization of (28) is not equal to the minimization of (26) but they share the same optimal solution. Based on the (28) one has

$$\begin{aligned} & \max_{w_k} \hat{r}(\theta) \\ &= \|[\tilde{A}^\theta, \tilde{B}^\theta]\|_F + \|\tilde{C}^\theta\|_F + L_g w_{max} + \|(\mathbf{Y} + w_{max})(\mathbf{G} + L_g w_{max})'\|_F \\ & \quad + \|(\bar{\mathbf{G}} + L_g w_{max}) \begin{bmatrix} \mathbf{G} \\ \mathbf{U} \end{bmatrix}'\|_F. \end{aligned} \quad (29)$$

Dropping the constant term of (29) one has the second layer minimization of (13) regarding to  $\theta \in \mathbb{R}^p$  as

$$\begin{aligned} & \min_{\theta \in \mathbb{R}^p} \hat{r}(\theta) \\ &= \min_{\theta \in \mathbb{R}^p} \|[\tilde{A}^\theta, \tilde{B}^\theta]\|_F + \|\tilde{C}^\theta\|_F + \|\mathbf{G}\|_F + \|\mathbf{G}\bar{\mathbf{G}}'\|_F. \end{aligned} \quad (30)$$

To sum up, we reduce the minimization problem of  $\min_{\theta_i} \max_{w_k} r(\theta_i, w)$  in (12) to  $\min_{\theta_i} \hat{r}(\theta_i)$  in (30). ■

## A.2 Simulation details

In this subsection, we first provide the simulation details regarding the experiment in Section 4, and then we present a detailed comparison between the proposed DKND and DKL methods.

	2D dynamics	Cartpole	Lunar lander	Surface vehicle
Optimizer	Adam			
Accuracy ( $\epsilon$ )	$1e-4$			
Training epochs ( $S$ )	1e4			
Learning rate ( $\alpha_i$ )	$1e-5$			
The number of data pairs (T)	500	600	1600	600
Loss function weight ( $\omega$ )	$0.5^i$	$0.5^i$	$0.6^i$	$0.6^i$
Compute resource	Apple M2, 16GB RAM			

Table 5: Training parameters.

### A.2.1 Computation resource and training parameters

### A.2.2 DNNs architecture

The DNN architectures of method DKND and DKL used in this paper are presented in Table 6. We refer to <https://pytorch.org/docs/stable/nn.html> for the definition of functions  $Linear()$ ,  $ReLU()$  and we denote  $layer^i$  as the  $i$ -th layer of the DNN and  $Linear([n, m])$  denotes a linear function with a weight matrix of shape  $n \times m$ . Since for the DKND and DKL methods, the input of

	2D dynamics	Cartpole	Lunar lander	Surface vehicle
layer <sup>1</sup> type	$Linear([2, 512])$	$Linear([4, 512])$	$Linear([6, 512])$	$Linear([6, 512])$
layer <sup>2</sup> type	$ReLU()$	$ReLU()$	$ReLU()$	$ReLU()$
layer <sup>3</sup> type	$Linear([512, 128])$	$Linear([512, 128])$	$Linear([512, 128])$	$Linear([512, 128])$
layer <sup>4</sup> type	$ReLU()$	$ReLU()$	$ReLU()$	$ReLU()$
layer <sup>5</sup> type	$Linear([128, 4])$	$Linear([128, 6])$	$Linear([128, 4])$	$Linear([128, 10])$

Table 6: DNN structures of DKND and DKL.

its DNN observable function is the measured state  $y_t$  and the input of the MLP method is a stacked vector of  $[y_t, u_t]'$  we show the DNNs structure of the MLP method in the following table.

	2D dynamics	Cartpole	Lunar lander	Surface vehicle
layer <sup>1</sup> type	$Linear([3, 512])$	$Linear([5, 512])$	$Linear([8, 512])$	$Linear([8, 512])$
layer <sup>2</sup> type	$ReLU()$	$ReLU()$	$ReLU()$	$ReLU()$
layer <sup>3</sup> type	$Linear([512, 128])$	$Linear([512, 128])$	$Linear([512, 128])$	$Linear([512, 128])$
layer <sup>4</sup> type	$ReLU()$	$ReLU()$	$ReLU()$	$ReLU()$
layer <sup>5</sup> type	$Linear([128, 4])$	$Linear([128, 6])$	$Linear([128, 4])$	$Linear([128, 10])$

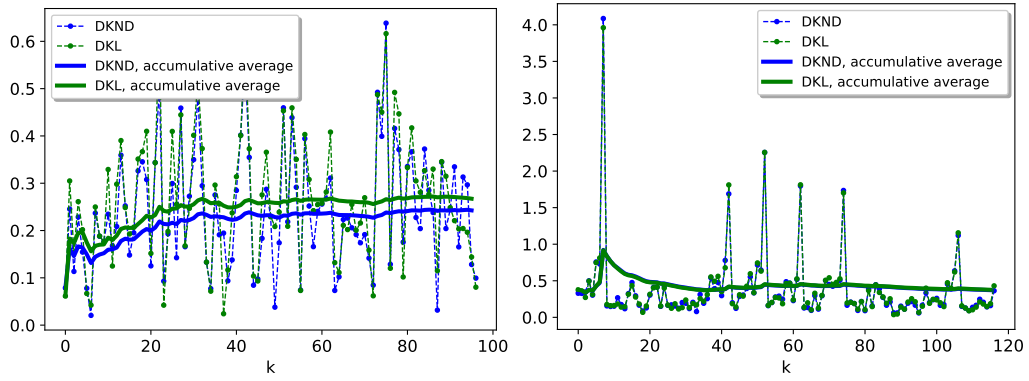
Table 7: DNN structures of MLP.

### A.3 Measurement noise generation

To experiment, we generate the Gaussian noise with mean  $\mu = 0$  and standard deviation  $\sigma = 2$ , the Poisson noise is generated with an expected separation  $\lambda = 3$ , and the uniform noise is generated from the open interval  $[-1, 2)$ . We refer to <https://numpy.org/doc/stable/reference/random/index.html> for more details of the noise generation. Note here that for any measurement noise  $w_t \in \mathbb{R}^n$  we transfer its upper bound from  $w_{max}$  to  $x_{max}$  by  $w_t := w_t * \frac{\max(x_t)}{\max(w_t)}$ ,  $t \in \{0, 1, \dots, T\}$ , where  $T$  is number of data pairs of (4).

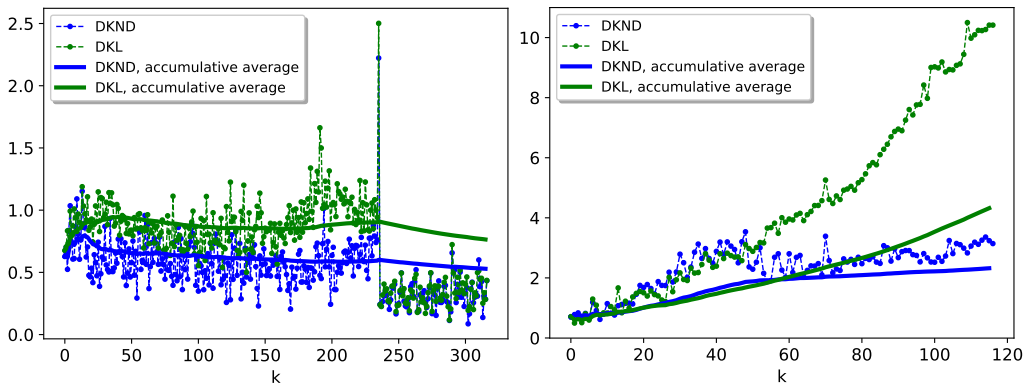
### A.4 Comparison between DKND and DKL

We show a detailed comparison between the DKND and DKL methods regarding the estimation errors in the following plots at one round experiment, where the dashed line denotes the estimation error  $\|e_{k+1}\|^2 = \|\hat{y}_{k+1} - x_{k+1}\|^2$  with  $\hat{y}_{k+1}$  being the output of the estimated dynamics given the  $(y_k, u_k)$  and  $x_{k+1}$  denotes the noise-free system state, and the solid line denotes the accumulative average of  $e_k$  defined as  $\frac{1}{k} \sum_{k=0}^k \|e_k\|^2$ .



(a) 2D dynamics.

(b) Cartpole



(c) Lunar Lander.

(d) Surface vehicle.

Figure 1: Gaussian noise.

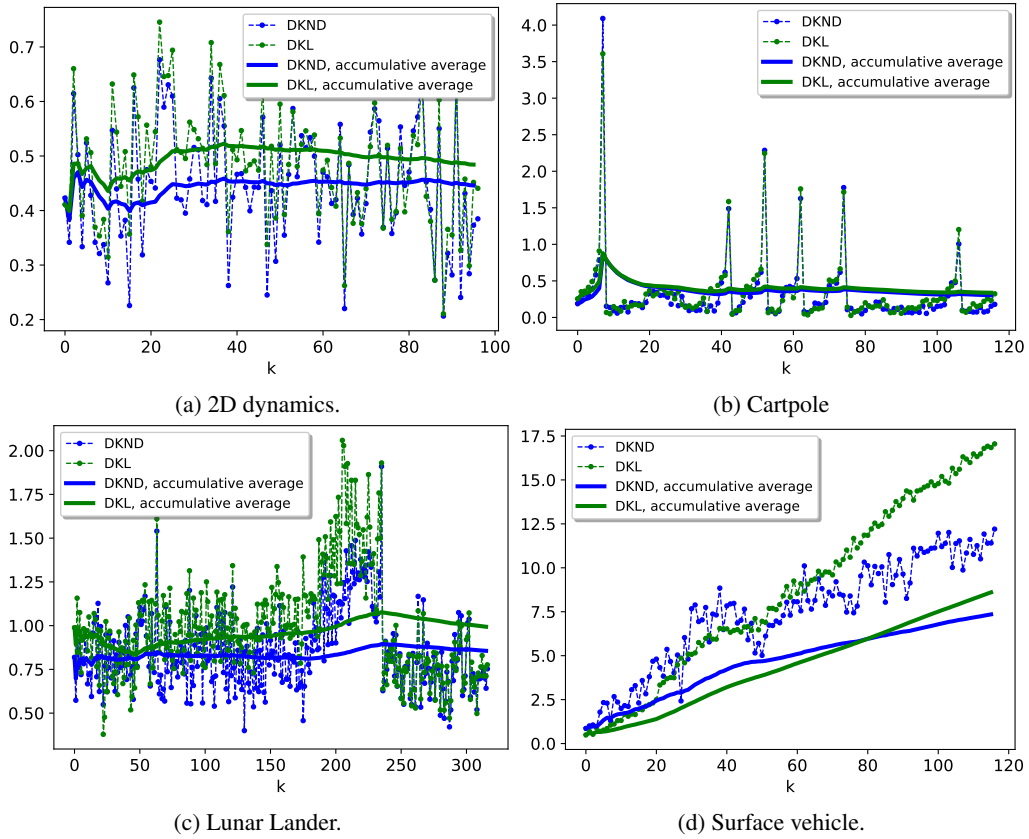


Figure 2: Poisson noise.

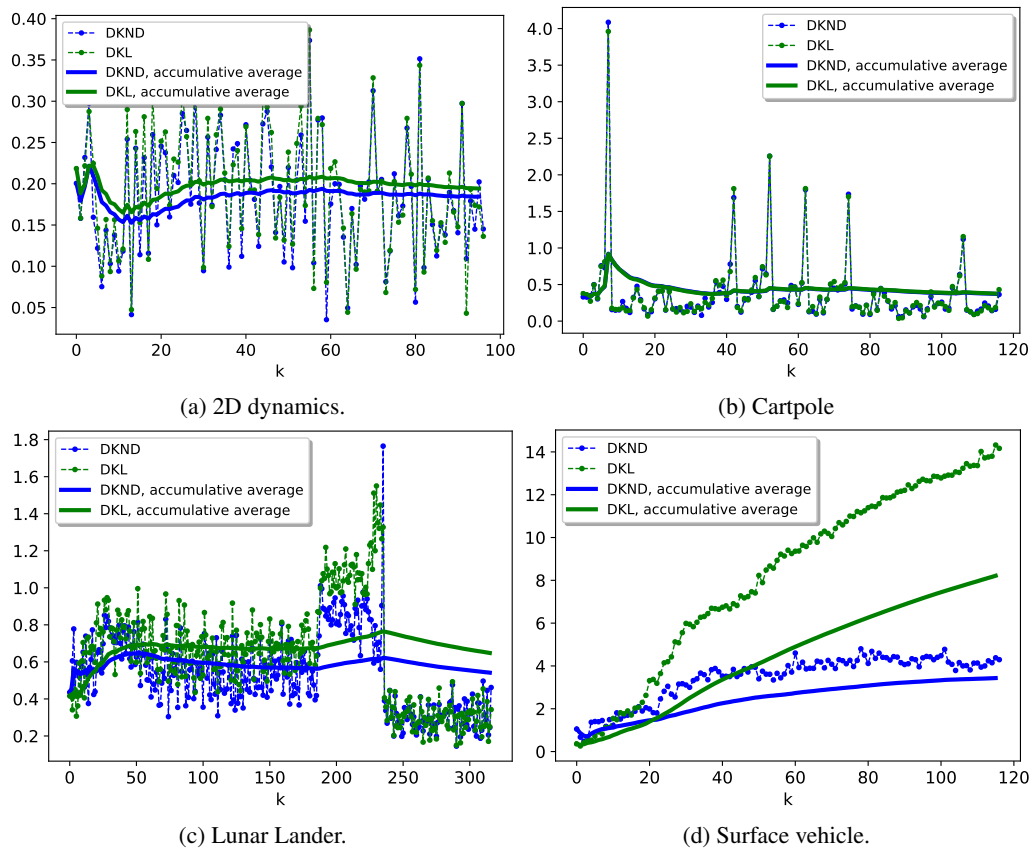


Figure 3: Uniform noise.